Earth Planet. Sci. Lett. 647 (2024) 119052

Contents lists available at ScienceDirect

Earth and Planetary Science Letters

journal homepage: www.elsevier.com/locate/epsl

Experimental investigation of hydrogen isotope fractionation during hydration of olivine-hosted melt inclusions: Implications for D/H in Baffin Island picrites

Yuxiang Zhang [a,b,c,*], Glenn Gaetani [a,*], Ayla Pamukçu [d], Brian Monteleone [a], Lee Saper [e,1]

[a] Department of Geology and Geophysics, Woods Hole Oceanographic Institution, Woods Hole, MA 02543, USA
[b] Key Laboratory of Ocean Observation and Forecasting, Key Laboratory of Marine Geology and Environment, Institute of Oceanology, Chinese Academy of Sciences, Qingdao, Shandong 266071, PR China
[c] Center for Ocean Mega-Science, Chinese Academy of Sciences, Qingdao, Shandong 266071, PR China
[d] Earth and Planetary Sciences, Stanford University, Stanford, CA 94306, USA
[e] School of Geosciences, Grant Institute, University of Edinburgh, EH9 3FE, UK

ARTICLE INFO

Editor: Fang-Zhen Teng

Keywords:
Melt inclusion
Olivine
Hydration
H^+ diffusivity
D/H
Volatile

ABSTRACT

Olivine-hosted melt inclusions are used to investigate the hydrogen isotope compositions (D/H) of Earth's mantle reservoirs. Studies have shown, however, that hydrogen in melt inclusion can equilibrate rapidly in response to changes to the external environment via the diffusion of protons (H^+) and deuterons (D^+) through the host olivine. Given that protons diffuse faster than deuterons, a kinetic fractionation of hydrogen isotopes is expected to accompany both the hydration and dehydration of melt inclusions. Other volatile species in the melt inclusion may also be affected by changes to the internal pressure and/or oxygen fugacity (fO_2). Here we report results from experiments designed to investigate the behaviors of volatiles and hydrogen isotopes during the hydration of olivine-hosted melt inclusions. We show that the concentration of H_2O in initially H_2O-poor inclusions increases rapidly (up to ~4 wt.% within 24 h) when the host olivine is in contact with aqueous fluid at 1200 °C and 300 MPa. The extent of hydration is controlled by time, temperature, melt inclusion volume, and H^+ diffusion distance. Hydrogen isotopes initially become lighter (i.e., D/H decreases) as hydration proceeds, defining a negative correlation with H_2O concentration. This trend reverses with increasing hydration as the inclusions must eventually equilibrate with the external fluid. These experimental results agree well with diffusion calculations carried out using a spherical geometry and a lattice diffusivity of $10^{-11.2\pm0.2}$ m^2/s for H^+ at 1200 °C. Therefore, anomalously light hydrogen isotopes in olivine-hosted melt inclusions from Baffin Island may not be taken as representative of the composition of the mantle source unless post-entrapment hydration can be excluded as a possibility. An increase in CO_2 concentration and a significant drop in sulfur concentration accompany hydration of the melt inclusions in our experiments. The former is consistent with an observed decrease in vapor bubble size and results from a hydration-induced internal pressure increase. The latter is ascribed to the exsolution of molten sulfide from the silicate melt, which might be related to a lower fO_2 in the experiments as compared to the starting materials. We find no evidence for exchange of F or Cl between the melt inclusion and external fluid.

1. Introduction

The isotopic composition of hydrogen [deuterium (D)/hydrogen (H)] has been used as a tool to investigate the origin of H_2O on Earth and H_2O exchange between Earth's surface and interior (e.g., Hallis et al., 2015; Poreda et al., 1986; Robert, 2001; Shaw et al., 2012). The origin of H_2O on Earth is still debated, where candidate sources have vastly different D/H, like protosolar nebular particulates ($\delta D_{VSMOW} = -870‰$; $\delta D_{VSMOW} = 1000 \times [(D/H)_{Sample}/ (D/H)_{VSMOW} - 1]$, where VSMOW is Vienna Standard Mean Ocean Water), comets (very high δD_{VSMOW}, up to +2400‰), and chondrites (intermediate δD_{VSMOW}) (Hallis et al., 2015; Piani et al., 2020). Determining Earth's original D/H signature is not

* Corresponding authors at: Department of Geology and Geophysics, Woods Hole Oceanographic Institution, Woods Hole, MA 02543, USA.
E-mail addresses: zhangyuxiang13@mails.ucas.ac.cn (Y. Zhang), ggaetani@whoi.edu (G. Gaetani).
[1] Current address: Jet Propulsion Laboratory, California Institute of Technology, Pasadena, CA 91125, USA

https://doi.org/10.1016/j.epsl.2024.119052
Received 21 June 2024; Received in revised form 19 September 2024; Accepted 26 September 2024
Available online 1 October 2024

only crucial to constrain the source of H_2O but can have important implications for the timing of H_2O accretion on our planet. Hallis et al. (2015) reported anomalously light hydrogen isotopes (δD_{VSMOW} = −218‰) in olivine-hosted melt inclusions from Baffin Island picrites, which was considered to have been sourced from an undegassed deep mantle that preserves Earth's initial D/H. Thus, they suggested this low D/H is evidence for the incorporation of protosolar-like H_2O during early Earth accretion.

Because the D/H of basaltic magma can be significantly modified during ascent from its mantle source region to the surface by processes such as degassing, magma mixing, and crustal assimilation, olivine-hosted melt inclusions are thought to preserve a more reliable record of the D/H signature of the mantle reservoir than do matrix glasses (e,g., Hallis et al., 2015; Kuritani et al., 2021; Shaw et al., 2008; Sobolev et al., 2019). Many studies, however, have demonstrated that olivine-hosted melt inclusions exhibit open system behavior with respect to protons (H^+), colloquially referred to as H_2O (e.g., Bucholz et al., 2013; Danyushevsky et al., 2002; Gaetani et al., 2012; Hartley et al., 2015; Hauri, 2002; Massare et al., 2002; Portnyagin et al., 2008). It is now well established that H_2O in olivine-hosted melt inclusions can rapidly equilibrate with the environment external to the host crystal via lattice diffusion of H^+ (Bucholz et al., 2013; Chen et al., 2011; Gaetani et al., 2012; Lloyd et al., 2013; Mironov et al., 2015; Portnyagin et al., 2008, 2019). Experimental studies have shown that D/H in olivine-hosted melt inclusions can significantly increase during dehydration, given that H^+ diffuses through olivine faster than deuterons (D^+) (Bucholz et al., 2013; Gaetani et al., 2012; Hauri, 2002).

Although in nature melt inclusion hydration is likely to be less common than dehydration, it could occur when the host melt gets mixed with a more hydrous melt (Hartley et al., 2015). Similar to the H isotope fractionation that occurs during dehydration, D/H is expected to fractionate during hydration, decreasing as the melt inclusion gains H_2O, which may produce anomalously low δD_{VSMOW}. In this case, light hydrogen isotopes found in the olivine-hosted melt inclusions would not reflect the composition of the mantle source. However, experimental constraints on the hydrogen isotope fractionation during the hydration of olivine-hosted melt inclusions are lacking. In addition, the behaviors of other volatile species (e.g., F, Cl, S, CO_2) during melt inclusion hydration remain unclear.

In this study, we report results from hydration experiments performed on olivine-hosted melt inclusions that elucidate the behaviors of volatiles and H isotopes during hydration ranging from 30 min to 24 h. Our results demonstrate significant H isotope fractionation as the melt inclusions diffusively gain H_2O from the external fluid. Extremely low δD_{VSMOW} was produced after short duration hydration. Thus, the low D/H in olivine-hosted melt inclusions from Baffin Island does not necessarily represent the source composition in deep Earth. The relative amount of H_2O gain is controlled by a combination of time, temperature (T), and the geometries of the melt inclusions and host olivines. Experimental hydration also influences the concentrations of some of the other volatile (e.g., CO_2) in the olivine-hosted melt inclusions.

2. Materials and methods

2.1. Starting materials

Hydration experiments were performed on natural olivine grains from Puu Mahana, south of Mauna Loa, Hawaii. These crystals were collected from an olivine-rich green sand beach that formed during erosion of nearby volcanic ash deposits (Walker, 1992). The olivine crystals contain abundant large, glassy melt inclusions, most of which contain a vapor bubble (Fig. S1). Analyses of twenty representative melt inclusions from the starting material that were not used in the experiments have consistently low H_2O contents (0.26 – 0.38 wt.%) but a range of δD_{VSMOW} values (−106.4 – −44.5‰), as well as CO_2 (in glass; 18 – 239 μg g^{-1}), S (467 – 1268 μg g^{-1}), F (247 – 339 μg g^{-1}), and Cl (46 – 79 μg g^{-1}) concentrations, after correction for post-entrapment crystallization (PEC) (Fig. S2). The PEC correction was performed using the olivine-melt equilibrium model of Beattie (1993) as implemented in the Petrolog3 software package (Danyushevsky and Plechov, 2011), which yields an equilibrium T (after PEC correction) of 1171 ± 30 °C (1 sd, N = 15) after correction for H_2O using the method of Médard and Grove (2008) (Table S1); this T is in agreement with the pre-eruptive T inferred for olivine-hosted MIs from the same location based on their MgO profiles (Saper and Stolper, 2020). Although we found that these melt inclusions have variable δD_{VSMOW} values, they are suitable as starting material for hydration experiments because the expected H isotope fractionation due to experimental hydration is so large (i.e., ~ 200 per mil variation). Additionally, the initial range of H_2O concentrations in the melt inclusions is small (variation ~0.1 wt.%) compared to that expected after hydration (up to ~4 wt.%; this study). This, in combination with the variable sizes of olivine crystals and melt inclusions, allows us to investigate the influences of the geometries of melt inclusions and their host crystals on the extent of diffusive hydration and the resulting time-varying changes in D/H.

2.2. Experimental methods

Experiments of various durations (30 min, 60 min, 90 min, and 24 h) were conducted at 1200 °C and 300 MPa. We used an end-loaded piston cylinder device (Boyd and England, 1960) with a 1.91 cm diameter assembly (Fig. S3) at Woods Hole Oceanographic Institution (WHOI). Twenty to twenty-five olivine grains containing melt inclusions were loaded into a thick-walled nickel capsule; ~80 μl of distilled H_2O (δD_{VSMOW} = 0.9 ± 0.5‰) (Mitchell et al., 2017) was added to the capsule using a microsyringe, and a nickel lid was placed on top. For the longest duration experiment (24 h), some powdered San Carlos olivine (<150 μm in diameter) was added to the capsule to minimize dissolution of olivine grains. The loaded nickel capsule was placed into concentric pyrophyllite and graphite sleeves, which were then centered in the hot spot of a straight-walled graphite furnace using crushable MgO spacers. Inclusion of the graphite sleeve produces a "stepped" furnace, minimizing the thermal gradient across the sample (Watson et al., 2002). The pressure medium for all experiments consisted of NaCl sleeves surrounding a Pyrex tube (e.g., Baker, 2004; Masotta et al., 2012; Mitchell et al., 2017; Moore et al., 2008). Pressure was calibrated using NaCl melting (Baker, 2004; Mitchell et al., 2017). Temperature was measured and controlled using a $W_3Re_{97}/W_{25}Re_{75}$ thermocouple. The reported T was not corrected for the effect of pressure (P) on thermocouple EMF. Temperature and P are estimated to be accurate to within ±10 °C and ±50 MPa, respectively. A stainless-steel base plug with a small extrusion was placed on top of the assembly (Fig. S3). During pressurization, the extrusion collapses, holding the thermocouple in place. The experiments were pressurized at room T and then heated at a rate of 60 °C/min. All experiments were terminated by shutting off the power. After each experiment, a hole was drilled through the nickel capsule to verify the presence of free water. Nickel oxide was not unambiguously identified inside the capsule after each experiment, indicating that the prevailing experimental oxygen fugacity (fO_2) might be lower than the nickel-nickel oxide (NNO) buffer (Faul et al., 2018).

2.3. Analytical methods

The radius of each recovered olivine grain was measured in three orthogonal directions along with the minimum distance from melt inclusion to olivine outer boundary using a SPOT Insight camera and imaging software, on a Nikon petrographic microscope, prior to mounting in epoxy. The radius of each melt inclusion was also measured in two orthogonal directions before it was exposed. Typical measurement errors for the olivine and inclusion radii are < 10 μm (1 sd) and < 1 μm (1 sd), respectively, which were estimated by repeating the measurements five times on each of five distinct crystals. After the melt

inclusions were exposed and polished, the olivine grains were removed from the epoxy mount and transferred into an indium metal mount to minimize volatile backgrounds during secondary ion mass spectrometry (SIMS) analyses. Volatile concentrations (H_2O, CO_2, F, Cl, and S) and hydrogen isotopic compositions of the melt inclusions were determined by SIMS using the Cameca IMS 1280 ion microprobe at the Northeast National Ion Microprobe Facility at WHOI. The concentrations of H_2O in the rims of the host olivine grains (as close to the edge as possible) from some 24 h hydration experiments were also measured to constrain the solubility of H_2O in olivine at our experimental conditions. The SIMS analytical method followed that reported by Bucholz et al. (2013) and Gaetani et al. (2014). A $^{133}Cs^+$ beam, with a primary current of 10 ± 0.5 nA (15 nA for H_2O in olivine) and an accelerating voltage of 10 kV, were used for SIMS analyses of both D/H and volatile concentrations. H and D were measured first. The mounts were then re-polished before measuring volatile concentrations on the same melt inclusions. The beam was rastered over a 30 × 30 μm area. The field aperture was set to be 406 × 406 μm for volatiles and 501 × 501 μm for D/H, blocking ions from beyond the innermost 5 – 6 μm^2 of the sputtering crater. This minimizes the contribution of "background" volatiles from the sample surface and within the sample chamber during analysis. Each measurement comprised a 240 s pre-sputtering period followed by 5 cycles of collection of ^{12}C, ^{16}OH, ^{19}F, ^{30}Si, ^{32}S, and ^{35}Cl with a mass resolving power (MRP) of ~6700 for volatiles or 20 cycles of collection of ^{16}OD and ^{16}OH with a MRP of ~9900 for D/H. Calibration for volatiles in melt inclusions was done using a series of basaltic glass standards (519–4–1, 46D, D52–5, D51–3, 1649–3, D20–3, JD17H, 6001, 1654–3, NS-1) and basaltic glass standard D52–5 for D/H (1 wt% H_2O, $\delta D_{VSMOW} = -51‰$). Olivine standards SCOH14 (15.8 μg g^{-1} H_2O), SCOH4 (39.2 μg g^{-1} H_2O), SCOH1 (55.6 μg g^{-1} H_2O), and SCOH7 (86.7 μg g^{-1} H_2O) (Gaetani et al., 2014) were used to calibrate the H_2O in olivine. Background corrections were done using analyses of nominally volatile-free materials (Suprasil SiO_2 glass and Synfo synthetic forsterite). The volatile concentrations and D/H of the standards and calibration curves for volatiles are given in Tables S2 to S4. Analytical precision on individual volatile concentration measurements is < 3% for CO_2 (2 sd) and < 2% (2 sd) for H_2O, F, S, and Cl. Uncertainties on calibration slopes, determined by bootstrap regression of standard measurement data, range from 2% – 6% (2 sd) among the volatiles for each session. $^{16}OD/^{16}OH$ was measured with a precision of 4‰ – 6‰ (2 rse). Standard reproducibility was ~7‰ – 10‰ (2 sd) during an analytical day.

After the SIMS measurements, the major element compositions of the melt inclusions and host olivine crystals were determined by electron microprobe (JEOL JXA-8200) at Massachusetts Institute of Technology (MIT). An accelerating voltage of 15 kV was used. For melt inclusion analyses, a 10 μm spot and a 10 nA beam current were adopted to reduce the migration of alkalis; counting times were 5 s for Na and 40 s for all other elements. A 1 μm spot size and a 30 nA beam current were used for olivine analyses; counting times were 300 s for Fe and 40 s for all other elements. Two to three measurements were done near the centers of

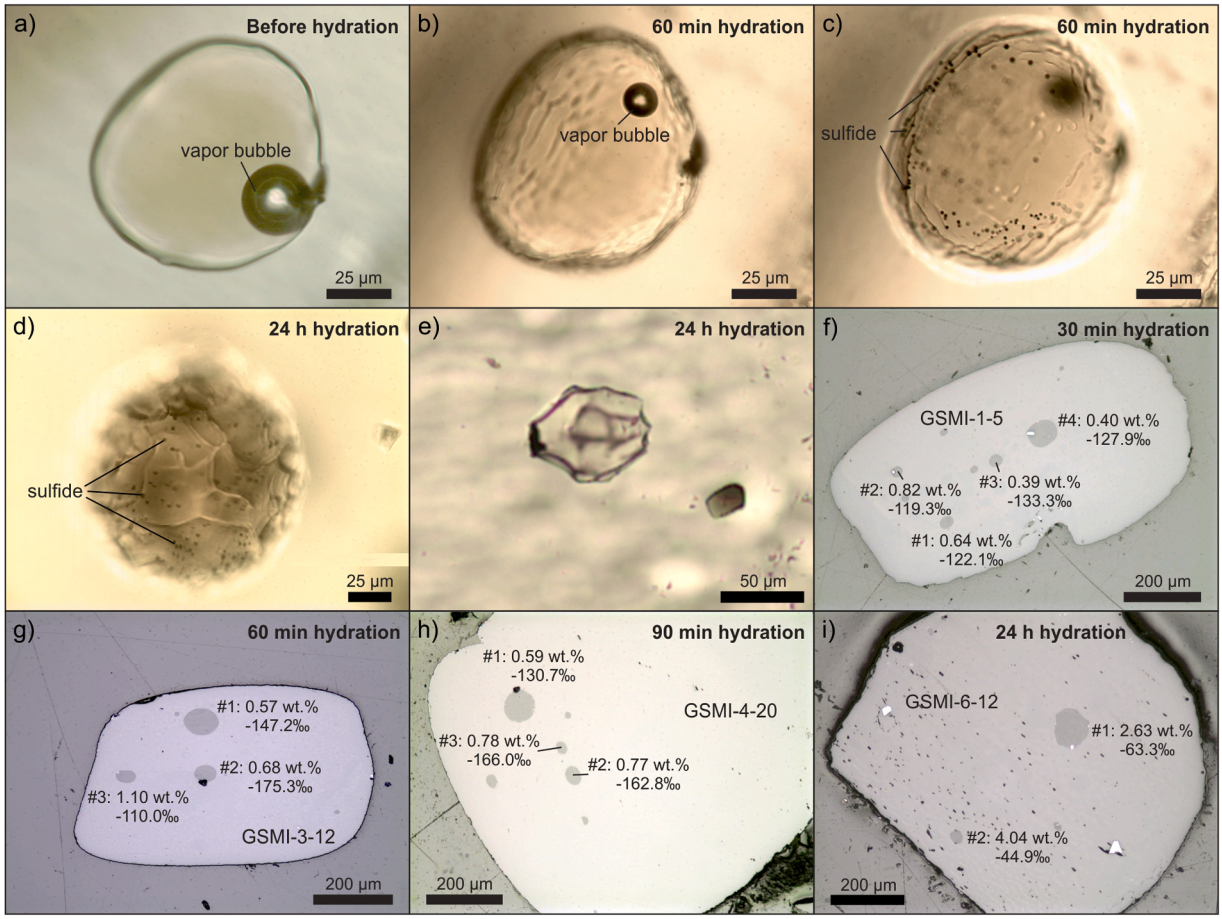

Fig. 1. Photomicrographs of Puu Mahana melt inclusions before (a) and after (b–i) hydration experiments conducted at 300 MPa and 1200 °C. (a) Olivine-hosted melt inclusion prior to hydration experiment. Note the large vapor bubble and smooth wall. (b, c) Melt inclusion in (a) after 60-min hydration experiment. Note that the vapor bubble is smaller, the inclusion wall is mottled, and sulfide globules (radius < 1 μm) exsolved from the melt. (d, e) Melt inclusions after 24-h hydration. The vapor bubble dissolved into the melt and the inclusion shapes became irregular; sulfide globules are present. (f–i) Reflected light photomicrographs showing H_2O concentrations (wt.%) and δD_{VSMOW} values (‰) of the inclusions hydrated for 30 min, 60 min, 90 min, and 24 h, respectively. For a single olivine, the inclusions that are smaller and/or closer to olivine outer boundary have higher H_2O contents.

each melt inclusion and five measurements were done for each host olivine. MORB glass Alvin1690–20 and olivine P140 were used as secondary standards.

3. Results

Compared with the unheated melt inclusions, the hydrated ones developed several new features. Firstly, inclusion walls became mottled (a "raisin" texture; Rose-Koga et al., 2021) after short hydration times (e.g., 60 min; Fig. 1b and c) and all the inclusion shapes became irregular after 24-h hydration (Fig. 1d and e). Secondly, the vapor bubbles decreased in size (Fig. 1b) and, following 24 h of hydration, disappeared (e.g., Figs. 1d and S1). In addition, the hydrated melt inclusions mostly contain abundant opaque globules (> 90% of them have radii smaller than 1 μm; Fig. 1c and d). Larger opaque globules enriched in S, Fe, and Ni are present in melt inclusions from the 24-h hydration experiment (Fig. S4). Thus, we conclude that opaque globules are quenched molten Fe-sulfide. In addition to sulfide globules, many melt inclusions in the 90-min and 24-h experiments contain daughter pyroxene crystals (< 2 μm to ~30 μm) (Figs. S5 and S6).

The hydrated melt inclusions in the four experimental groups (hydrated for 30 min, 60 min, 90 min, and 24 h) have similar size ranges, with the radii (average of two dimensions for each inclusion) in each group ranging from 15 μm to 60 μm. The radii of olivine crystals (average of three orthogonal directions for each crystal) in each group range from 200 μm to 700 μm, and the minimum distance from the edge of the inclusion to the outer surface of the olivine range from ~50 μm to ~350 μm. The size data are given in Table S1 and Fig. S7.

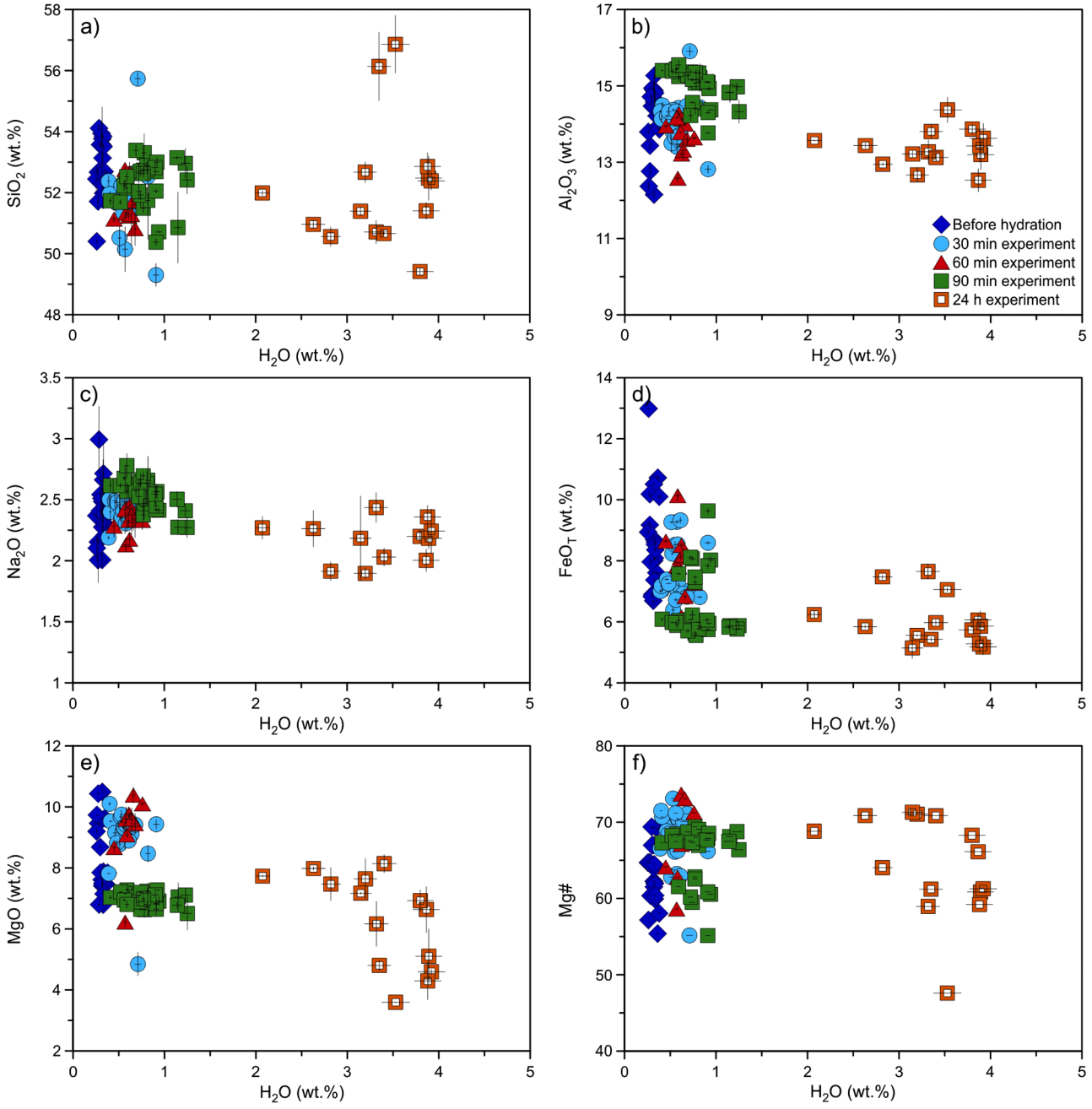

Fig. 2. Harker diagrams showing the variation of major element compositions of Puu Mahana melt inclusions before and after hydration. Error bars indicate 2 σ uncertainties. The compositions of the melt inclusions before hydration were corrected for post-entrapment crystallization (PEC). No correction was done on the hydrated melt inclusions.

Volatile concentrations, major element concentrations, and δD_{VSMOW} values of the melt inclusions and host olivines are also reported in Tables S1 and S5. The concentrations of the major oxides (except for FeO_T and MgO) are similar to the starting compositions. The 90-min and 24-h experiments have lower FeO_T and MgO concentrations on average than the short duration experiments and the starting materials (Fig. 2). This is likely due to crystallization of olivine on the inclusion walls and/or the daughter crystals in the melt inclusions (Fig. S5) in the longer duration runs, which is also reflected by the positive correlation between the concentration of H_2O and CIPW normative quartz (Fig. S8a) and the trend of increasing normative quartz with increasing hydration in the pseudoternary projection from plagioclase onto the clinopyroxene-olivine-quartz plane (Fig. S8b). Despite this, the range of Mg# seen in the hydrated groups is similar to that of the starting materials (Fig. 2f) and the FeO concentrations of the melt inclusions and their host crystals show positive linear correlations (Fig. S9), suggesting that the melt inclusions are in equilibrium with the host olivine during the crystallization differentiation.

The H_2O concentrations of the melt inclusions increase with experiment duration, reaching a maximum of ~4 wt.% after 24 h at 1200 °C and 300 MPa (Fig. 3). For each experiment, the H_2O concentrations span a range [30 min: 0.6 ± 0.1 wt.% (1 sd); 60 min: 0.7 ± 0.3 wt.%; 90 min: 0.8 ± 0.3 wt.%; 24 h: 3.5 ± 0.6 wt.%]; the inclusions with smaller volumes and/or shorter distances to the external olivine boundary tend to have higher H_2O concentrations (Figs. 1f-i and 4); this trend was not obvious for the small melt inclusions (radius < 30 μm) from the 24 h experiment, which may be close to equilibrium with the external fluid. The measured H_2O concentrations of the olivine rims range from 39 μg g^{-1} to 58 μg g^{-1}, with an average value of 49 μg g^{-1} (Table S5). The δD_{VSMOW} values of the hydrated melt inclusions also show a bit of variation [30 min: −129 ± 11‰ (1 sd); 60 min: −128 ± 23‰; 90 min: −149 ± 15‰; 24 h: −43 ± 16‰], but they tend to decrease progressively during the early stages of hydration (H_2O < 1 wt.%), eventually reaching an inflection point and then increasing with increasing H_2O concentrations, defining an asymmetric U-shaped curve, which projects towards the δD_{VSMOW} of the external fluid (Fig. 3).

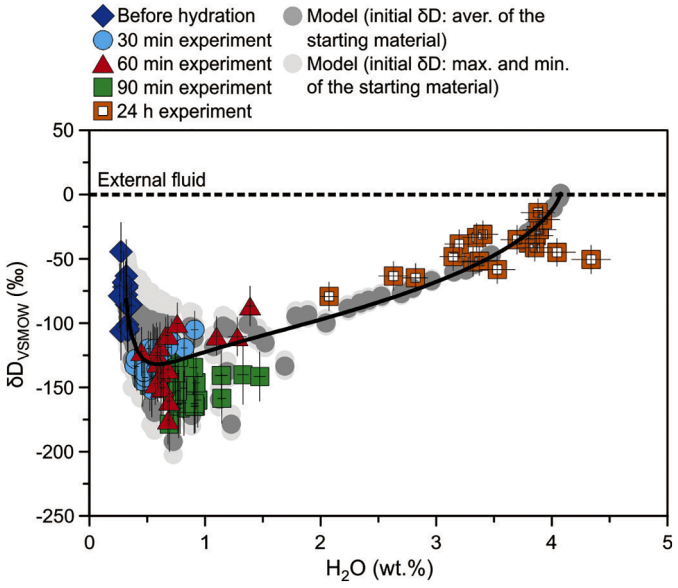

Fig. 3. δD_{VSMOW} values versus H_2O concentrations for the experimentally hydrated olivine-hosted melt inclusions showing the changes to δD_{VSMOW} values with increasing H_2O concentration for the melt inclusions in olivine in contact with aqueous fluid for 30 min, 60 min, 90 min, and 24 h. Error bars indicate 2 σ uncertainties for SIMS analyses. The model was formulated for a spherical geometry (Bucholz et al., 2013). The D^+ diffusivity was derived from Graham's law (β = 0.2) and a bulk H^+ diffusivity of $10^{-11.2}$ m^2/s at 1200 °C. The external boundary was set to aqueous fluid saturation in olivine (49 μg g^{-1}; this study) and the H_2O partition coefficient between olivine and silicate melt was set to be 0.0012 (Towbin et al., 2023 and this study). The black curve shows the variation of δD_{VSMOW} and H_2O concentration with time (0 to 100 h) for a single melt inclusion (inclusion radius = 25 μm; diffusion distance = 200 μm). The gray circles represent models that adopted the same geometries of inclusion and host olivine as those in the hydration experiments (inclusion radius = 15 to 60 μm; diffusion distance = 50 to 350 μm; t = 30 min, 60 min, 90 min, and 24 h). Each circle represents a specific melt inclusion radius and diffusion distance. A comparison between diffusion models with our experimental results for each run is shown in Fig. S12.

The concentration of CO_2 in the melt inclusion glass generally increases with increasing H_2O concentration. This results from resorption of the vapor bubbles as P within the melt inclusions increases as hydration proceeds [starting materials: 74.6 ± 58.8 μg g^{-1} (1 sd); 30 min: 131 ± 45 μg g^{-1}; 60 min: 207 ± 98 μg g^{-1}; 90 min: 150 ± 78 μg g^{-1}; 24 h: 198 ± 83 μg g^{-1}] (Fig. 5a). Conversely, the S concentrations of the hydrated inclusions are systematically lower than those of the majority of the original melt inclusions [starting materials: 978 ± 242 μg g^{-1} (1 sd); 30 min: 546 ± 199 μg g^{-1}; 60 min: 568 ± 219 μg g^{-1}; 90 min: 536 ± 90 μg g^{-1}; 24 h: 625 ± 109 μg g^{-1}] (Fig. 6a). No significant difference in S content was observed among the four experimental runs (Fig. 6a). The concentrations of F [30 min: 283 ± 34 μg g^{-1} (1 sd); 60 min: 271 ± 27 μg g^{-1}; 90 min: 310 ± 61 μg g^{-1}; 24 h: 328 ± 40 μg g^{-1}] and Cl [30 min: 56.1 ± 7.4 μg g^{-1} (1 sd); 60 min: 63.5 ± 21.3 μg g^{-1}; 90 min: 68.4 ± 9.3 μg g^{-1}; 24 h: 63.2 ± 10.9 μg g^{-1}] in the hydrated melt inclusions overlap with the distribution in the starting materials [F = 288 ± 25 μg g^{-1}; Cl = 61.5 ± 9.5 μg g^{-1}] (Fig. 7).

4. Discussion

4.1. Diffusive hydration of olivine-hosted melt inclusions

4.1.1. H^+ diffusivity in olivine equilibrating with aqueous fluid

Numerous studies have demonstrated that H_2O can be lost from olivine-hosted melt inclusions via the diffusion of H^+ (e.g., Barth et al., 2019; Bucholz et al., 2013; Chen et al., 2011, 2013; Gaetani et al., 2012; Hauri, 2002; Lloyd et al., 2013), which is evidenced by a negative correlation between δD_{VSMOW} and H_2O concentration resulting from H^+ diffusing faster than D^+ (Bucholz et al., 2013; Gaetani et al., 2012; Hauri, 2002). Other studies have shown that olivine-hosted melt inclusions can also rapidly gain H_2O from the external melt (e.g., Gaetani et al., 2012; Hartley et al., 2015; Mironov et al., 2015; Portnyagin et al., 2008, 2019). Portnyagin et al. (2008) suggested that the included melt gains H_2O via a combination of lattice diffusion of H^+ and transport of molecular H_2O along dislocation cores. However, Gaetani et al. (2012) used isotopically labelled water ($D_2^{18}O$) as the external fluid and found no elevated ^{18}O in either the hydrated melt inclusions or the interiors of host olivine grains but found increases in D, indicating that the included melt gains H_2O through the diffusion of D only.

The H^+ diffusion through olivine is largely controlled by the point defect population (e.g., Ferriss et al., 2018; Padrón-Navarta et al., 2014). While H_2O dissolves in silicate melt as a combination of hydroxyl groups and molecular H_2O, it is incorporated into – and diffuses through – olivine as H^+ and D^+ associated with metal vacancies, apparently leaving oxygen behind in the melt (Danyushevsky et al., 2002). However, Gaetani et al. (2012) showed that H_2O can be stoichiometrically (i.e., leaving no oxygen behind) incorporated into olivine according to the reaction:

$$H_2O_{fluid} + \frac{1}{2}[SiO_2]_{fluid} + Fe_{Me}^{\times} + 2O_O^{\times} = \left\{(OH)_O^{\bullet} - V^{''}_{Me} - (OH)_O^{\bullet}\right\}^{\times} + \frac{1}{2}Fe_2SiO_4 \quad (1)$$

where, in Kröger-Vink notation, $Fe_{Me}^{\times}$ is Fe^{2+}, occupying octahedral lattice sites, $O_O^{\times}$ and $(OH)_O^{\bullet}$ are O^{2-} and OH^-, respectively, occupying

oxygen sites, V''_{Me} is an octahedral site metal vacancy, and curly brackets indicate associated point defects (Kohlstedt and Mackwell, 1998). This equation can also be written for the Mg_2SiO_4 endmember of olivine.

We investigated the kinetics of melt inclusion hydration by comparing results from diffusion calculations with those from our experiments. The diffusion model of Bucholz et al. (2013), which is formulated using a spherical geometry with the melt inclusion located in the center of the olivine crystal, was used to estimate lattice diffusivity of H^+ and investigate relationships among diffusive gain of H_2O and the geometries of the melt inclusion and the host olivine during melt inclusion hydration. The sizes of the melt inclusions and the diffusion distances of H^+ (olivine radius minus melt inclusion radius) were informed by the hydration experiments (melt inclusion radius = 15, 20, 30, 40, 50, and 60 μm; diffusion distance = 50, 150, 250, and 350 μm; we used the minimum distance from the edge of the inclusion to the outer olivine surface to represent the diffusion distance in the modeling, because most of the melt inclusions are not centered in the host olivine). The average H_2O concentration of the starting melt inclusions (~0.3 wt. %) was used as the initial value. The outer boundary of the olivine grain was held at a constant H_2O concentration of 49 μg g^{-1} (the average value of the H_2O concentrations measured in the rim of hydrated olivine grains). Based on the updated H^+ partition coefficient between olivine and silicate melt (0.0009 ± 0.0003) (Towbin et al., 2023) and the measured values from olivine measurements close to the inclusions in our experiment (0.00112 to 0.00148; Fig. S10), the partition coefficient in the modeling was set to be 0.0012. For bulk H^+ diffusivities, we set a range of values ($10^{-11.0}$, $10^{-11.1}$, $10^{-11.2}$, $10^{-11.3}$, $10^{-11.4}$ m^2/s at 1200 °C) to determine the best match for our experimental results. Calculations were carried out using the MATLAB code of Bucholz et al. (2013). The results are shown in Fig. 4. For the inclusions with the same minimum diffusion distance, the H_2O concentrations in the inclusions increase progressively with decreasing inclusion radius (i.e., smaller inclusions have higher H_2O concentrations). For inclusions of similar size, those closer to the external olivine boundary tended to gain more H_2O. For all four groups of hydrated melt inclusions, the modeling results are most consistent with our experimental results using a bulk H^+ diffusivity of ~$10^{-11.2}$ m^2/s (at 1200 °C) (Fig. 4). The modeling results using other H^+ diffusivities ($10^{-11.1}$ and $10^{-11.3}$ m^2/s at 1200 °C) are not fully coincident with all four groups of experimental results (Fig. S11). Taking account of the variation of measured H_2O concentration in the olivine outer boundary (39 – 57 μg g^{-1}), the best estimated H^+ diffusivities at 1200 °C are between $10^{-11.0}$ and $10^{-11.4}$ m^2/s.

Our estimated bulk H^+ diffusivity (~$10^{-11.2\pm0.2}$ m^2/s at 1200 °C) is within the range of those previously estimated for randomly oriented olivines (~$10^{-11.5}$ – $10^{-10.5}$ m^2/s at 1200 °C) (Chen et al., 2011; Ferriss et al., 2018; Gaetani et al., 2012; Mironov et al., 2015; Portnyagin et al., 2008). In the hydration experiments of Portnyagin et al. (2019), a lower hydration efficiency for olivine-hosted melt inclusions (i.e., gaining less H_2O for the same experimental duration) was observed when the host olivine is in contact with aqueous fluid compared to that for silicate melt. They attributed this difference to a lower H^+ diffusivity in olivine in contact with a fluid (~$10^{-11.7}$ m^2/s at 1200 °C) relative to those in silicate melt (~10^{-11} m^2/s at 1200 °C). However, our estimated H^+ diffusivity is similar to the values when the olivine is in contact with silicate melt. This suggests that the difference in hydration efficiency of olivine-hosted melt inclusions between aqueous fluid and silicate melt is not a result of different H^+ diffusivity in olivine and requires further investigation.

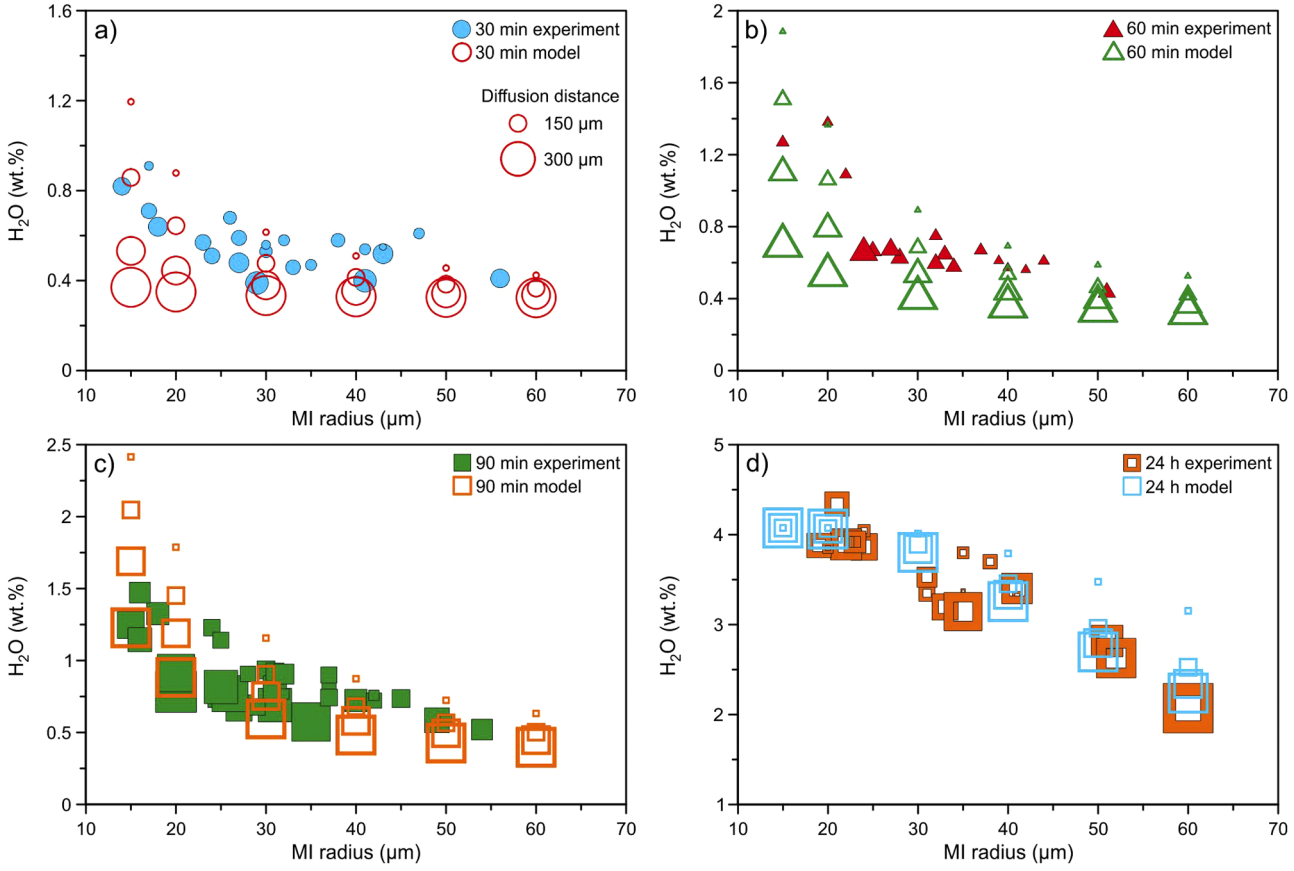

Fig. 4. Bubble diagrams showing the relationships among H_2O concentrations of melt inclusion, melt inclusion radius, and H^+ diffusion distance during the hydration of olivine-hosted melt inclusions, which were calculated from the H^+ diffusion model using the same parameters as in Fig. 3. The diffusion distance is reflected in the symbol size. The models best match our hydration experimental results using a bulk H^+ diffusivity of ~$10^{-11.2}$ m^2/s (at 1200 °C). The comparisons of our experimental results with diffusion models using other H^+ diffusivities ($10^{-11.1}$ and $10^{-11.3}$ m^2/s at 1200 °C) are shown in Fig. S11.

4.1.2. Hydrogen isotope fractionation

The variation of δD_{VSMOW} with H_2O concentration in our hydrated melt inclusions is consistent with the diffusive transport of H^+ from the external fluid into the inclusion. We used the diffusion model of Bucholz et al. (2013) to quantify the H isotope fractionation that develops during hydration. We assumed that the diffusivities (D_i) of protons and deuterons in olivine follow Graham's law of diffusion ($D_D^+/D_H^+ = (m_H/m_D)^\beta$, where m represents the mass number). We adopted a β value of 0.2 from Gaetani et al. (2012). The δD_{VSMOW} value of the external fluid was set at 0.9‰ (i.e., the δD_{VSMOW} value of our distilled water). The average (−81.1‰), maximum (−44.5‰), and minimum (−106.4‰) hydrogen isotope compositions of the starting melt inclusions were used as the initial δD_{VSMOW} values respectively to constrain the effect of variation of initial δD_{VSMOW} on the modeling results. Other parameters are the same as above, which consider the melt inclusion size and diffusion distance in the experiments. A forward model was calculated to show the variation of δD_{VSMOW} with increasing hydration for a single melt inclusion (inclusion radius = 25 μm; diffusion distance = 200 μm), using the average δD_{VSMOW} of the starting melt inclusions as the initial value.

Results from diffusion calculations for durations ranging from 30 min to 24 h are compared with our experimental results in Figs. 3 and S12. The results indicate that H_2O concentration increases monotonically with time, while the δD_{VSMOW} values initially decrease and then increase (Fig. 3). This pattern reflects the transient nature of the kinetic hydrogen isotope fractionation: the initial decrease of δD_{VSMOW} values is due to the faster diffusivity of H^+ than that of D^+. After the initial transient towards low δD_{VSMOW} values, as the bulk H_2O of the inclusion continues to equilibrate with the external melt, the D/H monotonically increases approaching the value in the external fluid.

Our experimental data plot mostly within the area defined by the modeling results (Figs. 3 and S12). In principle, the H isotope fractionation is also influenced by the size of the melt inclusion and the diffusion distance: for a given diffusion distance, smaller inclusions show larger isotopic fractionation during short hydration times (e.g., < 90 min) and equilibrate with the external melt faster. However, the relationships among H isotope fractionation, the melt inclusion size, and H^+ diffusion distance are difficult to define in our experiments because the δD_{VSMOW} values of the starting materials were not homogeneous (Fig. 3).

4.2. Implications for D/H in Baffin Island picrites

Hallis et al. (2015) reported anomalously light H isotopic compositions (δD_{VSMOW} = −218‰ to −97‰) for olivine-hosted melt inclusions in picritic basalts from Baffin Island, Canada. These picrites were erupted subaqueously and are naturally glassy. The δD_{VSMOW} values define a negative correlation with H_2O concentrations (H_2O = 576 to 1964 μg g^{-1}) in the melt inclusions. They concluded that the lightest H isotopic composition they measured (δD_{VSMOW} = −218‰) is the most indicative of the H isotope composition of the mantle source, which they inferred to be a mixture of protosolar-like deep mantle and mid-ocean ridge basalt (MORB) type upper mantle. They interpreted the negative correlation between the δD_{VSMOW} and H_2O concentration to be a result of melt inclusion dehydration during degassing (Bucholz et al., 2013; Gaetani et al., 2012). At these low H_2O contents (< 0.2 wt.%), however, an ascending magma would be expected to degas a vapor that is dominantly CO_2, although we cannot state that definitively because CO_2 was not measured. Nonetheless, if the Baffin picrites degas similarly to other H_2O-poor magmas, such as mid-ocean ridge basalts, they would have lost almost no H_2O and there would have been little-to-no driving force for dehydrating the Baffin Island melt inclusions (Dixon and Stolper, 1995; Dixon et al., 1995). Alternatively, if the eruption of the picrites was preceded by mixing with magma containing higher H_2O contents, the H_2O from the external melt would rapidly diffuse through the host olivine, hydrating the included melt and fractionating the hydrogen isotopes (Gaetani et al., 2012; Hartley et al., 2015; Mironov et al., 2015; Portnyagin et al., 2008).

The low H_2O concentrations (< 0.2 wt.%) that characterize the Baffin Island melt inclusions make them especially susceptible to modification by diffusive hydration (Hartley et al., 2015). Our results demonstrate that kinetic H isotope fractionation occurs during the initial stages of hydration of olivine-hosted melt inclusions, producing a negative correlation between δD_{VSMOW} and H_2O concentration and can produce anomalously low δD_{VSMOW} values (Fig. 3). This suggests that the low δD_{VSMOW} value (−218‰) reported by Hallis et al. (2015) may not represent the hydrogen isotopic composition of the mantle source. Alternatively, it can be an artifact of the inclusion-bearing olivine having been in contact with more H_2O-rich melt (e.g., ~0.8 wt.% H_2O) for >1–1.5 h prior to eruption and quenching (Fig. 8; the time estimate is a minimum based on a melt T of 1200 °C). Although such a relatively H_2O-rich melt has not yet been identified on Baffin Island, magmas containing ~1 wt.% H_2O have been reported elsewhere in the North Atlantic Igneous Province (e.g., Greenland) (Jamtveit et al., 2001).

We recognize that the mixing scenario proposed above requires a short timescale to preserve the observed hydrogen isotope fractionation (Fig. 8). Such a timescale could be achieved if the mixing occurred just prior to magma ascent and eruption. However, further work to better estimate the magma mixing timescale and magma ascent rate is needed to understand if hydration did affect the H isotope signature of the Baffin Island melt inclusions. Ultimately, we argue that our results imply that the low D/H in the Baffin Island olivine-hosted melt inclusions cannot be uniquely interpreted as representative of their mantle source unless diffusive hydration can be eliminated as a possibility.

4.3. Behaviors of other volatile species (CO_2, S, F, and Cl)

4.3.1. CO_2 dissolution

Determining the CO_2 concentrations in mineral-hosted melt inclusions is critical for understanding the flux of carbon from the mantle to the surface (e.g., Mironov et al., 2015; Shaw et al., 2010) as well as the depth of crystallization and melt inclusion entrapment (e.g., Hartley et al., 2014; Rasmussen et al., 2017; Wallace et al., 2015). However, most olivine-hosted melt inclusions contain a vapor bubble that sequesters a significant fraction of the total CO_2, in which case CO_2 estimates based only on glass measurements are always underestimates (as are the associated calculations of the P of vapor saturation) (Moore et al., 2015; Rasmussen et al., 2020; Wallace et al., 2015). Two methods have been developed to estimate the bulk CO_2 concentrations in bubble-bearing melt inclusions: (1) a mass balance method, which is a summation of CO_2 contents in glass and bubble; the latter is estimated using the volumes of the glass and the vapor bubble and the density of CO_2 in the bubble measured by Raman spectroscopy (e.g., Hartley et al., 2014; Moore et al., 2015); (2) a homogenization method, which attempts to dissolve the vapor bubbles back into the melt using high-pressure heating experiments (e.g., Hauri, 2002; Tuohy et al., 2016; Wallace et al., 2015). Mironov et al. (2015) used hydration experiments to homogenize melt inclusions in olivine crystals by completely dissolving vapor bubbles back into the melt, quenching it to a homogeneous glass, then analyzing the glass using SIMS or Fourier transform infrared spectroscopy (FTIR).

While the concentration of CO_2 in the hydrated melt inclusions is variable within each group of hydrated melt inclusions, there is a general increase as the melt inclusions gain H_2O during short duration hydration (≤ 90 min) (Fig. 5a). This is opposite to the direction observed in melt inclusion dehydration experiments (i.e., CO_2 decreases in the melt with increasing dehydration). The latter result has been ascribed to exsolution of CO_2 into vapor bubbles as a result of decreasing internal P during dehydration (Bucholz et al., 2013). Conversely, diffusive H_2O gain will increase the internal P due to an increase in the melt inclusion mass with essentially unchanged inclusion volume. As a result of the increased P due to H_2O gain, the CO_2 concentration increases with progressive hydration (Mironov et al., 2015). This is consistent with the shrinkage of vapor bubbles observed in the short duration hydrated melt

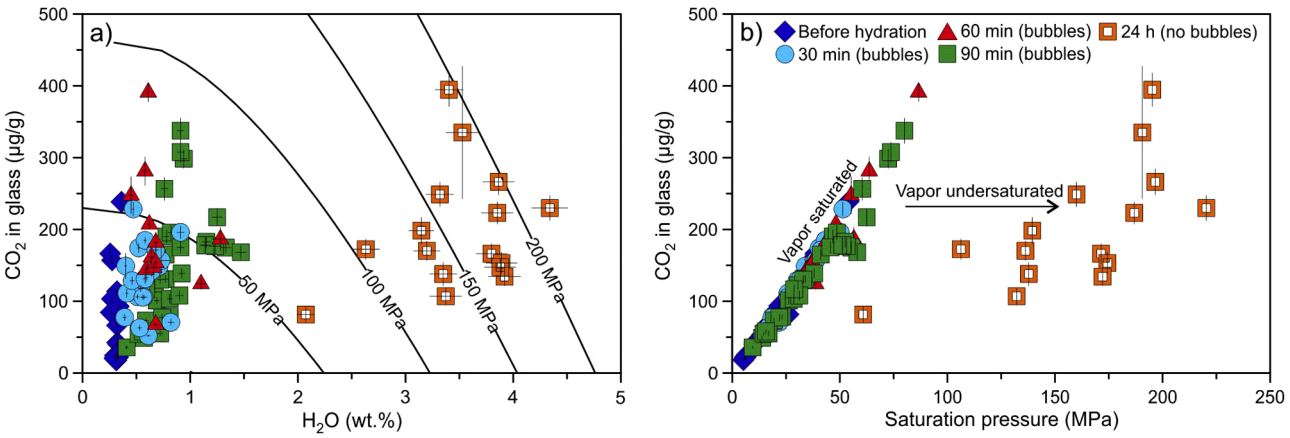

Fig. 5. Concentration of CO_2 in glass versus H_2O (a) and saturation P (b) in Puu Mahana olivine-hosted melt inclusions. Error bars indicate 2 σ uncertainties for SIMS analyses. The CO_2 concentrations of the melt inclusions before hydration were corrected for post-entrapment crystallization (PEC). The saturation P were calculated using VolatileCalc (Newman and Lowenstern, 2002). The CO_2 concentrations in the 24-h hydrated melt inclusions are not significantly increasing with increasing H_2O concentrations and saturation P, which is because these melt inclusions are vapor undersaturated, consistent with the absence of vapor bubbles.

inclusions (Fig. 1).

Note that the concentration of CO_2 in the 24-h hydrated melt inclusions was not significantly increasing with hydration (Fig. 5a). This may be in part due to the H_2O-suppression effect on CO_2 during SIMS analysis (Moussallam et al., 2024). However, we note that bubbles were not unambiguously identified in the 24-h hydrated melt inclusions (Fig. 1d and e; Table S1), indicating that the melt inclusions reached vapor undersaturation in < 24 h. Under these conditions, all the CO_2 was

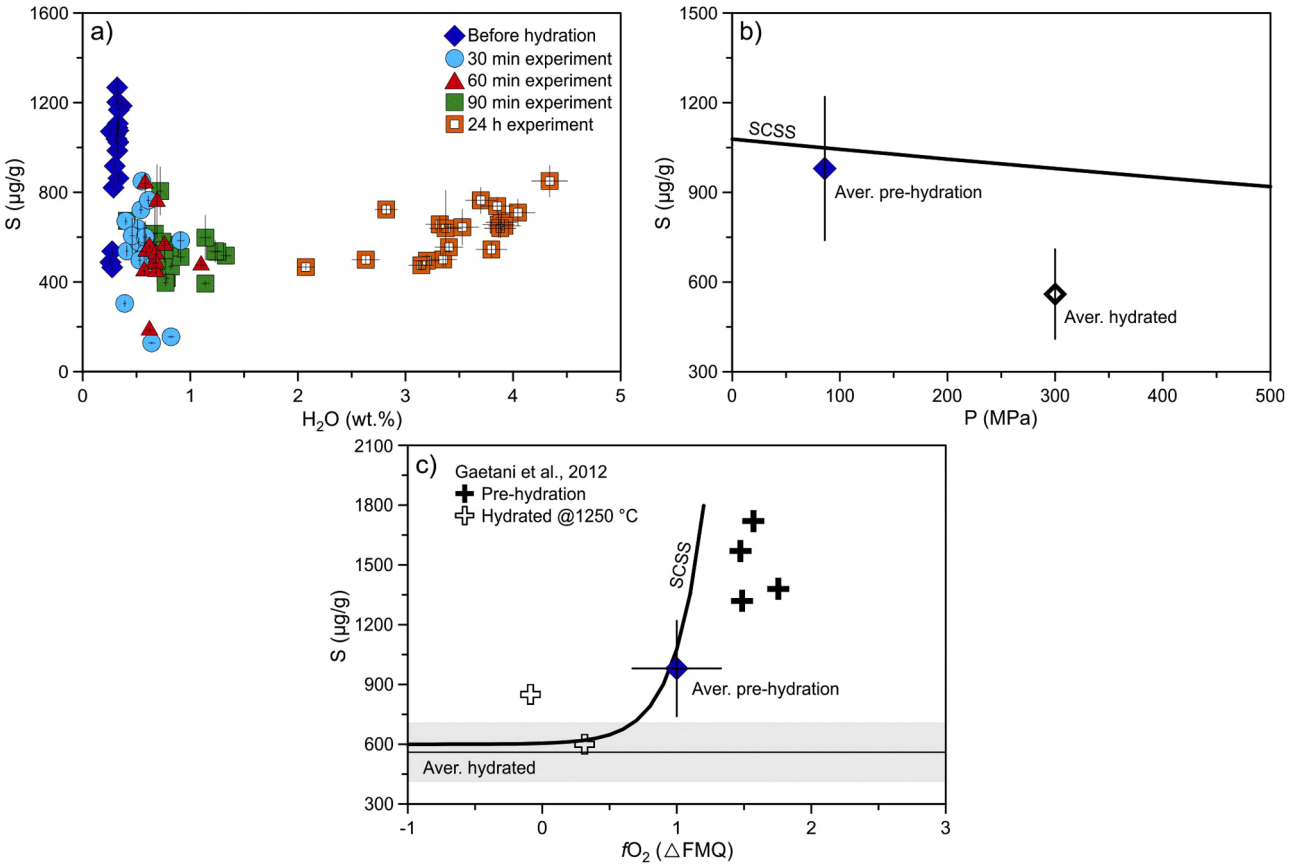

Fig. 6. (a) Plot of S versus H_2O in Puu Mahana olivine-hosted melt inclusions. (b) Comparison of sulfur in Puu Mahana melt inclusions with sulfide solubility. Vapor saturation pressures were calculated using VolatileCalc (Newman and Lowenstern, 2002) based on the concentrations of H_2O and CO_2 measured in melt inclusion glass. Pressures calculated for the 24 h experiments (vapor undersaturated) are minimum values. The black curve represents the S concentrations at sulfide solubility (SCSS) as a function of P calculated using the equation (10) of Mavrogenes and O'Neill (1999) for basalts without considering fO_2. (c) Influence of fO_2 on sulfide solubility. Hydration experimental data (1250 °C and 1 GPa) of Gaetani et al. (2012) are also presented. The fO_2 of the starting material in this study is according to Saper et al. (2024). The fO_2 relative to FMQ was calculated from $Fe^{3+}/\Sigma Fe$ using the methods of Borisov et al. (2018) and Frost (1991). The black curve represents the influence of fO_2 on SCSS calculated using the equation (10) of Jugo et al. (2010). The $SCSS^{2-}$ at low fO_2 was set to be 600 μg g^{-1}. The error bars indicate 2 σ uncertainty in (a, b) and 1 σ uncertainty in (c).

dissolved in the melt (vapor bubbles were gone). The vapor-undersaturated group can be clearly distinguished from vapor-saturated groups in the plots of CO_2 in glass versus calculated vapor saturation P (Fig. 5b). While the CO_2 concentrations in the 24-h hydrated melt inclusions may have been slightly affected by dilution (increasing H_2O concentration), they are comparable to those of Mauna Loa melt inclusions after homogenization (224 – 505 μg g^{-1}) (Wallace et al., 2015). Therefore, our experimental results confirm that hydration is an effective way to homogenize melt inclusions hosted in olivine (Mironov et al., 2015; Rasmussen et al., 2020).

4.3.2. Sulfide saturation

The concentrations of S in our experimentally hydrated melt inclusions (560 ± 150 μg g^{-1}) are systematically lower than those in melt inclusions from the starting material (980 ± 240 μg g^{-1}) (Fig. 6a). Three pristine melt inclusions from the starting material have low S concentrations (~500 – 600 μg g^{-1}), which reflects the heterogeneous S concentrations of the Mauna Loa magmas (Davis et al., 2003). However, these low-S melt inclusions only account for ~15% of the pristine inclusions we analyzed. Therefore, we suggest the S concentrations in the melt inclusions decreased significantly during hydration. We interpret this decrease to reflect exsolution of molten sulfide from the silicate melt, which is supported by the presence of sulfide globules in our experiments (Fig. 1c and d).

The sulfur concentration at sulfide saturation (SCSS) in silicate melt is influenced by T, P, oxygen fugacity (fO_2), H_2O content, and melt composition (specifically Fe concentration) (e.g., Baker and Moretti, 2011; Fortin et al., 2015; Holzheid and Grove, 2002; Jugo et al., 2005; Li and Ripley, 2009; Liu et al., 2007; Mavrogenes and O'Neill, 1999; Nash et al., 2019). In our case, a change of melt composition has little influence on the SCSS because the FeO concentration in the hydrated melt inclusions from the 30 and 60 min experiments are similar to those in the pristine melt inclusions (Fig. 2d). Melt H_2O concentrations might play a role in the decrease of sulfur concentration, although the influence of H_2O on the SCSS is the subject of debate. Results from some studies suggest that the SCSS decreases with increasing H_2O concentration in the melt (e.g., Li and Ripley, 2009; Liu et al., 2007; Moretti and Baker, 2008), while others indicate a positive correlation between the SCSS and H_2O concentration (e.g., Fortin et al., 2015; Moune et al., 2009). The S concentrations in our melt inclusions show no significant correlation with H_2O concentrations for our hydrated melt inclusions (Fig. 6a). Furthermore, the formation of sulfide globules in some experimentally dehydrated olivine-hosted melt inclusions (Mironov et al., 2015; Saper and Stolper, 2020) suggests that the exsolution of sulfides is not related to high H_2O concentrations in the melt.

Experiments have shown that increasing P can decrease the SCSS in silicate melt (Holzheid and Grove, 2002; Mavrogenes and O'Neill, 1999). Nevertheless, this influence is poorly constrained at lower P (< 1 GPa) (O'Neill, 2021). Using the model of Mavrogenes and O'Neill (1999) that shows significant effect of P on SCSS at 0 – 1 GPa, an increase of P by 300 MPa can only lead to a decrease of SCSS by < 100 μg g^{-1} (Fig. 6b). This further excludes P as a major driving force for the formation of sulfide blebs. The sulfide blebs could form during quench due to the effect on sulfide solubility of lowering T (e.g., Ding et al., 2018). While the quench rate in our experiments was not measured, the quench rate for a typical piston cylinder experiment is ~130 °C/s (Ezad et al., 2023), which is much higher than the natural eruptive cooling rate for Hawaii lavas (100s to 10000s °C/hr) (Saper and Stolper, 2020). If cooling plays a major role in the sulfide saturation, more sulfide blebs and lower S concentrations would be expected in natural olivine-hosted melt inclusions in Puu Mahana, which, however, is not consistent with the observations (Figs. 1a and 6a). This suggests that cooling is not a major controlling factor on the sulfide exsolution.

Oxygen fugacity plays an important role in stabilizing sulfide through its control of the oxidation state of S in silicate melt (S^{2-} or sulfide versus S^{6+} or sulfate) over a narrow range of fO_2 (FMQ to FMQ+2, where FMQ is the fayalite-magnetite-quartz buffer) and results in much lower S solubility in silicate melt at lower fO_2 (Baker and Moretti, 2011; Jugo et al., 2005; Wallace and Carmichael, 1994). Recent studies have shown that the fO_2 of olivine-hosted melt inclusions can rapidly equilibrate with changes to the external environment (e.g., Bucholz et al., 2013; Gaetani et al., 2012; Hartley et al., 2017). Although the fO_2 conditions were not well constrained in our experiments, rapid reduction during high P hydration of olivine-hosted melt inclusions has also been reported in previous experiments (e.g., Gaetani et al., 2012; Taracsák et al., 2023). For example, in the hydration experiment of Gaetani et al. (2012), the $Fe^{3+}/\Sigma Fe$ of olivine-hosted melt inclusions from Mauna Loa decreased from 0.21 – 0.25 to 0.16 – 0.19 after 22- to 48-h hydration at 1250 °C and 1 Gpa. The reduction of S^{6+} to S^{2-} at low fO_2 would promote sulfide saturation, lowering the concentration of S in the melt phase, which is consistent with the decrease of S concentrations in the hydrated melt inclusions compared to the starting materials (from 1320 – 1720 μg g^{-1} to 600 – 850 μg g^{-1}) (Fig. 6c). According to the Fe XANES (X-ray absorption near edge structure spectroscopy) measurements of Puu Mahana melt inclusions (Saper et al., 2024), the Puu Mahana melt inclusions have a $Fe^{3+}/\Sigma Fe$ of 0.15 – 0.21, corresponding to FMQ+0.6 to FMQ+1.4 (Borisov et al., 2018; Frost, 1991). Sulfur XANES measurements of these melt inclusions all yielded mixed S^{6+} and S^{2-} ($S^{6+}/\Sigma S = 0.35 – 0.94$) (Saper et al., 2024). This is consistent with the majority of the starting melt inclusions being sulfide undersaturated despite their higher S concentrations; upon experimental reduction sulfide saturation was achieved forming the sulfide blebs (Fig. 6c). Note that based on the appearance of ubiquitous sulfides in the 30 min experiments, reduction appears to have occurred rapidly.

Therefore, fO_2 may play a critical role in the exsolution of sulfide blebs during melt inclusion hydration, although the potential effects of H_2O, P, and quench cannot be eliminated. Our results imply that a sulfide-saturated melt inclusion can potentially be used to investigate or test the influences of fO_2, P, or T on the sulfide solubility in silicate melt, providing that other factors can be well constrained.

4.3.3. F and Cl

It is debatable whether melt inclusions in olivine are a closed system with respect to F. In the dehydration experiments of Bucholz et al. (2013), there were no significant changes to F concentrations in the melt inclusions that were dehydrated for up to 68 h, suggesting no diffusive migration of F through the host olivine. For our hydration experiments, the F concentrations among the hydrated inclusions are nearly constant and comparable to the concentrations in our pristine inclusions (Fig. 7a), which supports the suggestion that F was not diffusively equilibrated with the external aqueous fluid.

Conversely, Portnyagin et al. (2008) reported a significant loss of F from their experimentally hydrated melt inclusions and attributed it to a diffusive migration of F through the host olivine. Post-entrapment F enrichment was also observed in some natural olivine-hosted melt inclusions, and it was ascribed to the presence of F-clinohumite lamellae in the olivine structure that act as fast diffusion pathways for F (Koleszar et al., 2009). Further, an increase of F concentration in the host olivine towards the melt inclusion was found in some natural olivine crystals (Le Voyer et al., 2014). We note that all the olivine grains that recorded F mobility in these studies were in contact with silicate melts, rather than aqueous fluid (this study) or gas (Bucholz et al., 2013). One possible explanation for these differences, therefore, is that the external boundary condition may influence the behavior of F in olivine-hosted melt inclusions. Since F partitions into the melt relative to fluid or gas (e.g., Aiuppa et al., 2009), the only case in which there is a driving force for diffusive loss or gain of F is perhaps when the olivine is surrounded by melt. If that is the case, olivine-hosted melt inclusions would be an open system for F in nature when the external boundary is a melt.

Cl mobility in olivine has not been observed. The Cl concentrations in our hydrated melt inclusions behave similarly to F (Fig. 7b) and are consistent with the results of dehydration experiments (Bucholz et al.,

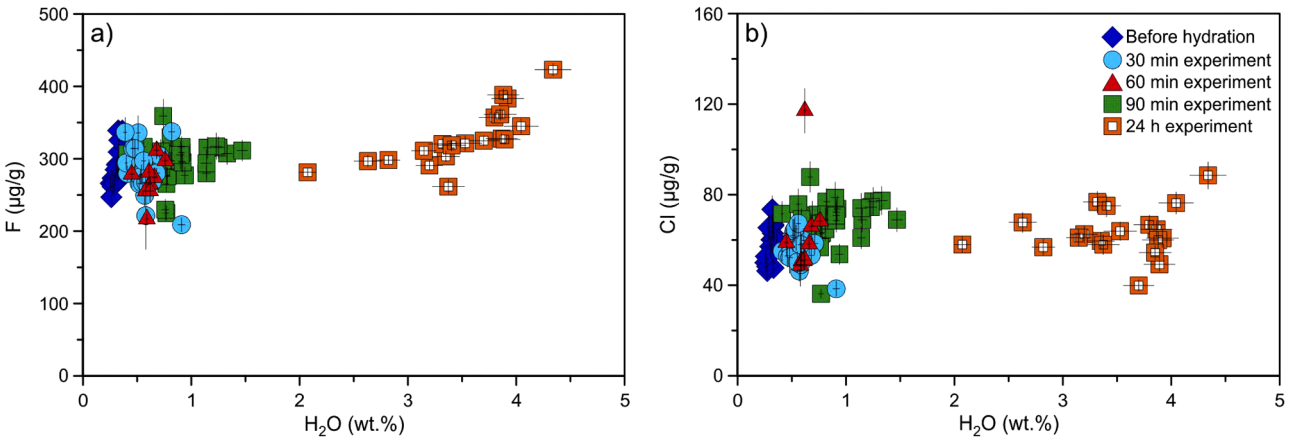

Fig. 7. Plots of H_2O versus F (a) and Cl (b) in Puu Mahana olivine-hosted melt inclusions.

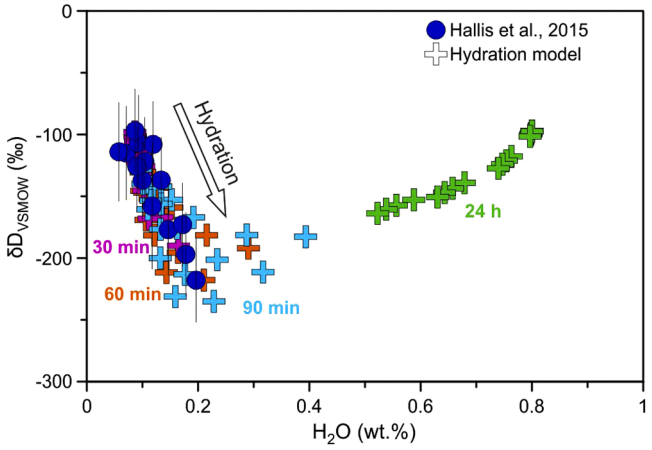

Fig. 8. Modeling results for the H^+ diffusion showing the covariation of δD_{VSMOW} values and H_2O concentrations for the Baffin Island melt inclusions (H_2O = 0.086 wt.%; δD_{VSMOW} = −97‰; radius = 15 – 50 μm) after the host olivines (radius = 200 – 500 μm) contact with a slightly more hydrous melt (H_2O = 0.8 wt.%) with the same hydrogen isotope for 30 min to 24 h. Baffin Island melt inclusion data reported by Hallis et al. (2015) are also shown for comparison (error bars: 2 σ). The model used the same parameters as in Fig. 3. The modeling results agree well with the natural data, suggesting that anomalously light hydrogen isotopes in the olivine-hosted melt inclusion can be produced via hydration and do not necessarily represent the hydrogen isotopic composition of deep mantle source.

2013). This indicates that olivine-hosted melt inclusions are a closed system with respect to Cl, at least when external boundary is fluid or gas.

5. Conclusions

Results from hydration experiments with durations ranging from 30 min to 24 h demonstrate that olivine-hosted melt inclusions can rapidly gain H_2O from the external environment via diffusion of H^+ through the host olivine. The smaller melt inclusions and/or those closer to the edge of the olivine gain H_2O more rapidly. The H isotope composition became transiently lighter in short duration hydration experiments (< 1 h), which could mimic the situation for olivine crystals in contact with a more H_2O-rich melt during magma mixing. Therefore, anomalously light δD_{VSMOW} values, such as those measured in Baffin picrites, may reflect a diffusive transient rather than the δD_{VSMOW} of a primitive, undegassed mantle source. Our experimental data also show that the H^+ diffusivity in olivine equilibrated with an aqueous fluid (about $10^{-11.2\pm0.2}$ m^2/s at 1200 °C) is faster than previously estimated values under similar external environment (i.e., aqueous fluid) and approaches that for equilibration with a hydrous silicate melt. In addition, hydration increases the internal P of the melt inclusion, resulting in the dissolution of CO_2 from vapor bubbles into the melt. Furthermore, the S concentrations in the hydrated melt inclusions dropped significantly as a result of exsolution of sulfide globules, likely due to the decrease of oxygen fugacity imposed by the experimental assembly and reduction of S^{6+} initially dissolved in the melt inclusions. This implies that olivine-hosted melt inclusions are a potential tool to probe the effects of redox conditions, T, or P on the sulfide solubility in silicate melt. Similar to dehydration experiments, no exchange of F and Cl between the melt inclusion and external aqueous fluid was observed in our hydration experiment.

CRediT authorship contribution statement

Yuxiang Zhang: Writing – original draft, Methodology, Investigation, Formal analysis, Data curation. **Glenn Gaetani:** Writing – review & editing, Supervision, Methodology, Funding acquisition, Conceptualization. **Ayla Pamukçu:** Writing – review & editing, Investigation, Formal analysis. **Brian Monteleone:** Writing – review & editing, Methodology, Data curation. **Lee Saper:** Writing – review & editing, Investigation, Formal analysis.

Declaration of competing interest

The authors declare that they have no known competing financial interests or personal relationships that could have appeared to influence the work reported in this paper.

Data availability

Data will be made available on request.

Acknowledgements

We are grateful to Horst Marschall for providing olivines from Puu Mahana, Hawaii. We also thank Terry Plank for comments on an earlier version of the paper and Rajdeep Dasgupta and Fangzhen Teng for their editorial handling and suggestions. This work was supported by the US National Science Foundation (NSF OCE-2135901) to G.G. Y.Z. acknowledges the support from the National Key Research and Development Program of China (2023YFF0804304 and 2023YFF0804301) and the National Natural Science Foundation of China (42206058, 42330409, and 42221005).

Supplementary materials

Supplementary material associated with this article can be found, in the online version, at doi:10.1016/j.epsl.2024.119052.

References

Aiuppa, A., Baker, D.R., Webster, J.D., 2009. Halogens in volcanic systems. Chem. Geol. 263, 1–18.

Baker, D.R., 2004. Piston-cylinder calibration at 400 to 500 MPa: a comparison of using water solubility in albite melt and NaCl melting. Am. Mineral. 89, 1553–1556.

Baker, D.R., Moretti, R., 2011. Modeling the solubility of sulfur in magmas: a 50-year old geochemical challenge. Rev. Mineral. Geochem. 73, 167–213.

Barth, A., Newcombe, M., Plank, T., Gonnermann, H., Hajimirza, S., Soto, G.J., Saballos, A., Hauri, E., 2019. Magma decompression rate correlates with explosivity at basaltic volcanoes — constraints from water diffusion in olivine. J. Volcanol. Geotherm. Res. 387, 106664.

Beattie, P., 1993. Olivine-melt and orthopyroxene-melt equilibria. Contrib. Mineral. Petrol. 115, 103–111.

Borisov, A., Behrens, H., Holtz, F., 2018. Ferric/ferrous ratio in silicate melts: a new model for 1 atm data with special emphasis on the effects of melt composition. Contrib. Mineral. Petrol. 173, 98.

Boyd, F.R., England, J.L., 1960. Apparatus for phase-equilibrium measurements at pressures up to 50 kgbars and temperatures up to 1750 °C. J. Geophys. Res. 65, 741–748.

Bucholz, C.E., Gaetani, G.A., Behn, M.D., Shimizu, N., 2013. Post-entrapment modification of volatiles and oxygen fugacity in olivine-hosted melt inclusions. Earth Planet Sci. Lett. 374, 145–155.

Chen, Y., Provost, A., Schiano, P., Cluzel, N., 2011. The rate of water loss from olivine-hosted melt inclusions. Contrib. Mineral. Petrol. 162, 625–636.

Chen, Y., Provost, A., Schiano, P., Cluzel, N., 2013. Magma ascent rate and initial water concentration inferred from diffusive water loss from olivine-hosted melt inclusions. Contrib. Mineral. Petrol. 165, 525–541.

Danyushevsky, L.V., McNeill, A.W., Sobolev, A.V., 2002. Experimental and petrological studies of melt inclusions in phenocrysts from mantle-derived magmas: an overview of techniques, advantages and complications. Chem. Geol. 183, 5–24.

Danyushevsky, L.V., Plechov, P., 2011. Petrolog3: integrated software for modeling crystallization processes. Geochem. Geophys. Geosyst. 12, Q07021.

Davis, M.G., Garcia, M.O., Wallace, P., 2003. Volatiles in glasses from Mauna Loa Volcano, Hawai'i: implications for magma degassing and contamination, and growth of Hawaiian volcanoes. Contrib. Mineral. Petrol. 144, 570–591.

Ding, S., Hough, T., Dasgupta, R., 2018. New high pressure experiments on sulfide saturation of high-FeO* basalts with variable TiO_2 contents – Implications for the sulfur inventory of the lunar interior. Geochim. Cosmochim. Acta 222, 319–339.

Dixon, J.E., Stolper, E.M., 1995. An experimental study of water and carbon dioxide solubilities in mid-ocean ridge basaltic liquids. Part II: applications to degassing. J. Petrol. 36, 1633–1646.

Dixon, J.E., Stolper, E.M., Holloway, J.R., 1995. An experimental study of water and carbon dioxide solubilities in mid-ocean ridge basaltic liquids. Part I: calibration and solubility models. J. Petrol. 36, 1607–1631.

Ezad, I.S., Shcheka, S.S., Buhre, S., Buhre, A., Gorojovsky, L.R., Shea, J.J., Förster, M.W., Foley, S.F., 2023. Rapid quench piston cylinder apparatus: an improved design for the recovery of volatile-rich geological glasses from experiments at 0.5–2.5 GPa. Rev. Sci. Instrum. 94, 055107.

Faul, U.H., Cline Ii, C.J., Berry, A., Jackson, I., Garapić, G., 2018. Constraints on oxygen fugacity within metal capsules. Phys. Chem. Miner. 45, 497–509.

Ferriss, E., Plank, T., Newcombe, M., Walker, D., Hauri, E., 2018. Rates of dehydration of olivines from San Carlos and Kilauea Iki. Geochim. Cosmochim. Acta 242, 165–190.

Fortin, M.-A., Riddle, J., Desjardins-Langlais, Y., Baker, D.R., 2015. The effect of water on the sulfur concentration at sulfide saturation (SCSS) in natural melts. Geochim. Cosmochim. Acta 160, 100–116.

Frost, B.R., 1991. Introduction to oxygen fugacity and its petrologic importance. In: Donald, H.L. (Ed.), Oxide Minerals. De Gruyter, Berlin, Boston, pp. 1–10.

Gaetani, G.A., O'Leary, J.A., Koga, K.T., Hauri, E.H., Rose-Koga, E.F., Monteleone, B.D., 2014. Hydration of mantle olivine under variable water and oxygen fugacity conditions. Contrib. Mineral. Petrol. 167, 965.

Gaetani, G.A., O'Leary, J.A., Shimizu, N., Bucholz, C.E., Newville, M., 2012. Rapid reequilibration of H_2O and oxygen fugacity in olivine-hosted melt inclusions. Geology 40, 915–918.

Hallis, L.J., Huss, G.R., Nagashima, K., Taylor, G.J., Halldórsson, S.A., Hilton, D.R., Mottl, M.J., Meech, K.J., 2015. Evidence for primordial water in Earth's deep mantle. Science 350, 795–797.

Hartley, M.E., Maclennan, J., Edmonds, M., Thordarson, T., 2014. Reconstructing the deep CO_2 degassing behaviour of large basaltic fissure eruptions. Earth Planet Sci. Lett. 393, 120–131.

Hartley, M.E., Neave, D.A., Maclennan, J., Edmonds, M., Thordarson, T., 2015. Diffusive over-hydration of olivine-hosted melt inclusions. Earth Planet Sci. Lett. 425, 168–178.

Hartley, M.E., Shorttle, O., Maclennan, J., Moussallam, Y., Edmonds, M., 2017. Olivine-hosted melt inclusions as an archive of redox heterogeneity in magmatic systems. Earth Planet Sci. Lett. 479, 192–205.

Hauri, E.H., 2002. SIMS analysis of volatiles in silicate glasses, 2: isotopes and abundances in Hawaiian melt inclusions. Chem. Geol. 183, 115–141.

Holzheid, A., Grove, T.L., 2002. Sulfur saturation limits in silicate melts and their implications for core formation scenarios for terrestrial planets. Am. Mineral. 87, 227–237.

Jamtveit, B., Brooker, R., Brooks, K., Larsen, L.M., Pedersen, T., 2001. The water content of olivines from the North Atlantic Volcanic Province. Earth Planet Sci. Lett. 186, 401–415.

Jugo, P.J., Luth, R.W., Richards, J.P., 2005. Experimental data on the speciation of sulfur as a function of oxygen fugacity in basaltic melts. Geochim. Cosmochim. Acta 69, 497–503.

Jugo, P.J., Wilke, M., Botcharnikov, R.E., 2010. Sulfur K-edge XANES analysis of natural and synthetic basaltic glasses: implications for S speciation and S content as function of oxygen fugacity. Geochim. Cosmochim. Acta 74, 5926–5938.

Kohlstedt, D.L., Mackwell, S.J., 1998. Diffusion of hydrogen and intrinsic point defects in olivine. Z. Phisikalische Chem. 207, 147–162.

Koleszar, A.M., Saal, A.E., Hauri, E.H., Nagle, A.N., Liang, Y., Kurz, M.D., 2009. The volatile contents of the Galapagos plume; evidence for H_2O and F open system behavior in melt inclusions. Earth Planet Sci. Lett. 287, 442–452.

Kuritani, T., Shimizu, K., Ushikubo, T., Xia, Q.-K., Liu, J., Nakagawa, M., Taniuchi, H., Sato, E., Doi, N., 2021. Tracing the subducting Pacific slab to the mantle transition zone with hydrogen isotopes. Sci. Rep. 11, 18755.

Le Voyer, M., Asimow, P.D., Mosenfelder, J.L., Guan, Y., Wallace, P.J., Schiano, P., Stolper, E.M., Eiler, J.M., 2014. Zonation of H_2O and F concentrations around melt inclusions in olivines. J. Petrol. 55, 685–707.

Li, C., Ripley, E.M., 2009. Sulfur contents at sulfide-liquid or anhydrite saturation in silicate melts: empirical equations and example applications. Econ. Geol. 104, 405–412.

Liu, Y., Samaha, N.-T., Baker, D.R., 2007. Sulfur concentration at sulfide saturation (SCSS) in magmatic silicate melts. Geochim. Cosmochim. Acta 71, 1783–1799.

Lloyd, A.S., Plank, T., Ruprecht, P., Hauri, E.H., Rose, W., 2013. Volatile loss from melt inclusions in pyroclasts of differing sizes. Contrib. Mineral. Petrol. 165, 129–153.

Masotta, M., Freda, C., Paul, T.A., Moore, G.M., Gaeta, M., Scarlato, P., Troll, V.R., 2012. Low pressure experiments in piston cylinder apparatus: calibration of newly designed 25mm furnace assemblies to P=150MPa. Chem. Geol. 312–313, 74–79.

Massare, D., Métrich, N., Clocchiatti, R., 2002. High-temperature experiments on silicate melt inclusions in olivine at 1 atm: inference on temperatures of homogenization and H_2O concentrations. Chem. Geol. 183, 87–98.

Mavrogenes, J.A., O'Neill, H.S.C., 1999. The relative effects of pressure, temperature and oxygen fugacity on the solubility of sulfide in mafic magmas. Geochim. Cosmochim. Acta 63, 1173–1180.

Médard, E., Grove, T.L., 2008. The effect of H_2O on the olivine liquidus of basaltic melts: experiments and thermodynamic models. Contrib. Mineral. Petrol. 155, 417–432.

Mironov, N., Portnyagin, M., Botcharnikov, R., Gurenko, A., Hoernle, K., Holtz, F., 2015. Quantification of the CO_2 budget and H_2O–CO_2 systematics in subduction-zone magmas through the experimental hydration of melt inclusions in olivine at high H_2O pressure. Earth Planet Sci. Lett. 425, 1–11.

Mitchell, A.L., Gaetani, G.A., O'Leary, J.A., Hauri, E.H., 2017. H_2O solubility in basalt at upper mantle conditions. Contrib. Mineral. Petrol. 172, 85.

Moore, G., Roggensack, K., Klonowski, S., 2008. A low-pressure–high-temperature technique for the piston-cylinder. Am. Mineral. 93, 48–52.

Moore, L.R., Gazel, E., Tuohy, R., Lloyd, A.S., Esposito, R., Steele-MacInnis, M., Hauri, E. H., Wallace, P.J., Plank, T., Bodnar, R.J., 2015. Bubbles matter: an assessment of the contribution of vapor bubbles to melt inclusion volatile budgets. Am. Mineral. 100, 806–823.

Moretti, R., Baker, D.R., 2008. Modeling the interplay of fO_2 and fS_2 along the FeS-silicate melt equilibrium. Chem. Geol. 256, 286–298.

Moune, S., Holtz, F., Botcharnikov, R.E., 2009. Sulphur solubility in andesitic to basaltic melts: implications for Hekla volcano. Contrib. Mineral. Petrol. 157, 691–707.

Moussallam, Y., Towbin, W.H., Plank, T., Bureau, H., Khodja, H., Guan, Y., Ma, C., Baker, M.B., Stolper, E.M., Naab, F.U., Monteleone, B.D., Gaetani, G.A., Shimizu, K., Ushikubo, T., Lee, H.J., Ding, S., Shi, S., Rose-Koga, E.F., 2024. ND70 series basaltic glass reference materials for volatile element (H_2O, CO_2, S, Cl, F) measurement and the C ionisation efficiency suppression effect of water in silicate glasses in SIMS. Geostand. Geoanal. Res. https://doi.org/10.1111/ggr.12572.

Nash, W.M., Smythe, D.J., Wood, B.J., 2019. Compositional and temperature effects on sulfur speciation and solubility in silicate melts. Earth Planet Sci. Lett. 507, 187–198.

Newman, S., Lowenstern, J.B., 2002. VolatileCalc: a silicate melt–H_2O–CO_2 solution model written in visual basic for excel. Comput. Geosci. 28, 597–604.

O'Neill, H.S.C., 2021. The thermodynamic controls on sulfide saturation in silicate melts with application to ocean floor basalts. In: Moretti, R., Neuville, D.R. (Eds.), Magma Redox Geochemistry. American Geophysical Union, Washington DC, pp. 177–213.

Padrón-Navarta, J.A., Hermann, J., O'Neill, H.S.C., 2014. Site-specific hydrogen diffusion rates in forsterite. Earth Planet Sci. Lett. 392, 100–112.

Piani, L., Marrocchi, Y., Rigaudier, T., Vacher, L.G., Thomassin, D., Marty, B., 2020. Earth's water may have been inherited from material similar to enstatite chondrite meteorites. Science 369, 1110–1113.

Poreda, R., Schilling, J.G., Craig, H., 1986. Helium and hydrogen isotopes in ocean-ridge basalts north and south of Iceland. Earth Planet Sci. Lett. 78, 1–17.

Portnyagin, M., Almeev, R., Matveev, S., Holtz, F., 2008. Experimental evidence for rapid water exchange between melt inclusions in olivine and host magma. Earth Planet Sci. Lett. 272, 541–552.

Portnyagin, M., Mironov, N., Botcharnikov, R., Gurenko, A., Almeev, R.R., Luft, C., Holtz, F., 2019. Dehydration of melt inclusions in olivine and implications for the origin of silica-undersaturated island-arc melts. Earth Planet Sci. Lett. 517, 95–105.

Rasmussen, D.J., Kyle, P.R., Wallace, P.J., Sims, K.W.W., Gaetani, G.A., Phillips, E.H., 2017. Understanding degassing and transport of CO_2-rich alkalic magmas at Ross Island, Antarctica using olivine-hosted melt inclusions. J. Petrol. 58, 841–861.

Rasmussen, D.J., Plank, T.A., Wallace, P.J., Newcombe, M.E., Lowenstern, J.B., 2020. Vapor-bubble growth in olivine-hosted melt inclusions. Am. Mineral. 105, 1898–1919.
Robert, F., 2001. The origin of water on Earth. Science 293, 1056–1058.
Rose-Koga, E.F., Bouvier, A.S., Gaetani, G.A., Wallace, P.J., Allison, C.M., Andrys, J.A., Angeles de la Torre, C.A., Barth, A., Bodnar, R.J., Bracco Gartner, A.J.J., Butters, D., Castillejo, A., Chilson-Parks, B., Choudhary, B.R., Cluzel, N., Cole, M., Cottrell, E., Daly, A., Danyushevsky, L.V., DeVitre, C.L., Drignon, M.J., France, L., Gaborieau, M., Garcia, M.O., Gatti, E., Genske, F.S., Hartley, M.E., Hughes, E.C., Iveson, A.A., Johnson, E.R., Jones, M., Kagoshima, T., Katzir, Y., Kawaguchi, M., Kawamoto, T., Kelley, K.A., Koornneef, J.M., Kurz, M.D., Laubier, M., Layne, G.D., Lerner, A., Lin, K. Y., Liu, P.P., Lorenzo-Merino, A., Luciani, N., Magalhães, N., Marschall, H.R., Michael, P.J., Monteleone, B.D., Moore, L.R., Moussallam, Y., Muth, M., Myers, M.L., Narváez, D.F., Navon, O., Newcombe, M.E., Nichols, A.R.L., Nielsen, R.L., Pamukcu, A., Plank, T., Rasmussen, D.J., Roberge, J., Schiavi, F., Schwartz, D., Shimizu, K., Shimizu, K., Shimizu, N., Thomas, J.B., Thompson, G.T., Tucker, J.M., Ustunisik, G., Waelkens, C., Zhang, Y., Zhou, T., 2021. Silicate melt inclusions in the new millennium: a review of recommended practices for preparation, analysis, and data presentation. Chem. Geol. 570, 120145.
Saper, L.M., Baker, M.B., Brounce, M., Hughes, E.C., Hofmann, A.E., Stolper, E.M., 2024. Experimental constraints on iron and sulfur redox equilibria and kinetics in basaltic melt inclusions. Geochim. Cosmochim. Acta 381, 75–96.
Saper, L.M., Stolper, E.M., 2020. Controlled cooling-tate experiments on olivine-hosted melt inclusions: chemical diffusion and quantification of eruptive cooling rates on Hawaii and Mars. Geochem. Geophys. Geosyst. 21, e2019GC008772.
Shaw, A.M., Behn, M.D., Humphris, S.E., Sohn, R.A., Gregg, P.M., 2010. Deep pooling of low degree melts and volatile fluxes at the 85 °E segment of the Gakkel Ridge: evidence from olivine-hosted melt inclusions and glasses. Earth Planet Sci. Lett. 289, 311–322.
Shaw, A.M., Hauri, E.H., Behn, M.D., Hilton, D.R., Macpherson, C.G., Sinton, J.M., 2012. Long-term preservation of slab signatures in the mantle inferred from hydrogen isotopes. Nat. Geosci. 5, 224–228.
Shaw, A.M., Hauri, E.H., Fischer, T.P., Hilton, D.R., Kelley, K.A., 2008. Hydrogen isotopes in Mariana arc melt inclusions: implications for subduction dehydration and the deep-Earth water cycle. Earth Planet Sci. Lett. 275, 138–145.
Sobolev, A.V., Asafov, E.V., Gurenko, A.A., Arndt, N.T., Batanova, V.G., Portnyagin, M. V., Garbe-Schönberg, D., Wilson, A.H., Byerly, G.R., 2019. Deep hydrous mantle reservoir provides evidence for crustal recycling before 3.3 billion years ago. Nature 571, 555–559.
Taracsák, Z., Mather, T.A., Ding, S., Plank, T., Brounce, M., Pyle, D.M., Aiuppa, A., 2023. Sulfur from the subducted slab dominates the sulfur budget of the mantle wedge under volcanic arcs. Earth Planet Sci. Lett. 602, 117948.
Towbin, W.H., Plank, T., Klein, E., Hauri, E., 2023. Measuring H_2O concentrations in olivine by secondary ion mass spectrometry: challenges and paths forward. Am. Mineral. 108, 928–940.
Tuohy, R.M., Wallace, P.J., Loewen, M.W., Swanson, D.A., Kent, A.J.R., 2016. Magma transport and olivine crystallization depths in Kīlauea's east rift zone inferred from experimentally rehomogenized melt inclusions. Geochim. Cosmochim. Acta 185, 232–250.
Walker, G.P.L., 1992. Puu Mahana near South Point in Hawaii is a primary Surtseyan ash ring, not a sandhills-type littoral cone. Pac. Sci. 46, 1–10.
Wallace, P.J., Carmichael, I.S.E., 1994. S speciation in submarine basaltic glasses as determined by measurements of SKα X-ray wavelength shifts. Am. Mineral. 79, 161–167.
Wallace, P.J., Kamenetsky, V.S., Cervantes, P., 2015. Melt inclusion CO_2 contents, pressures of olivine crystallization, and the problem of shrinkage bubbles. Am. Mineral. 100, 787–794.
Watson, E., Wark, D., Price, J., Van Orman, J., 2002. Mapping the thermal structure of solid-media pressure assemblies. Contrib. Mineral. Petrol. 142, 640–652.